AD-A235 477

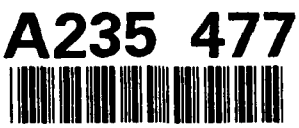

(2)

TATION PAGE

Form Approved
OMB No. 0704-0188

1. AGENCY USE ONLY (Leave blank)	2. REPORT DATE	3. REPORT TYPE AND DATES COVERED
	March 1991	Reprint

4. TITLE AND SUBTITLE

Electric Potential patterns Deduced for the SUNDIAL Period of September 23-26, 1986

5. FUNDING NUMBERS

61102F 2310 A2

6. AUTHOR(S)

See Back

7. PERFORMING ORGANIZATION NAME(S) AND ADDRESS(ES)

SRI International
333 Ravenswood Avenue
Menlo Park, CA 94025-3493

AFOSR-TR- 91 0466

8. PERFORMING ORGANIZATION REPORT NUMBER

9. SPONSORING/MONITORING AGENCY NAME(S) AND ADDRESS(ES)

AFOSR/NC
Building 410, Bolling AFB DC
20332-6448

10. SPONSORING/MONITORING AGENCY REPORT NUMBER

F49620-87-K-0007

11. SUPPLEMENTARY NOTES

Annales Geophysicae, 1990, 8, (6), 399-408

12a. DISTRIBUTION/AVAILABILITY STATEMENT

APPROVED FOR PUBLIC RELEASE; DISTRIBUTION IS UNLIMITED

12b. DISTRIBUTION CODE

13. ABSTRACT (Maximum 200 words)

ABSTRACT High-latitude electric potential and ionospheric conductance patterns are presented and discussed for the Northern Hemisphere during the SUNDIAL period of September 23-26, 1986 using the Assimilative Mapping of Ionospheric Electrodynamics (AMIE) technique of Richmond and Kamide (1988). Data sources used for the model are satellite and ground magnetometers, electron precipitation instruments, incoherent scatter radars, and ionospheric coherent radars. The period was characterized by many substorms, and a wide variety of instantaneous patterns of electrodynamic parameters on a hemispheric scale are derived throughout this period, of which only a few examples are displayed. The entire set of electric potentials and conductances are being made available through the NCAR CEDAR Data Base for further analysis and utilization in simulation models.

14. SUBJECT TERMS

15. NUMBER OF PAGES
10

16. PRICE CODE

17. SECURITY CLASSIFICATION OF REPORT	18. SECURITY CLASSIFICATION OF THIS PAGE	19. SECURITY CLASSIFICATION OF ABSTRACT	20. LIMITATION OF ABSTRACT
UNCLASSIFIED	UNCLASSIFIED	UNCLASSIFIED	SAR

AD-A235 477

TATION PAGE

Form Approved
OMB No. 0704-0188

1. AGENCY USE ONLY (Leave blank)	2. REPORT DATE	3. REPORT TYPE AND DATES COVERED
	March 1991	Reprint

4. TITLE AND SUBTITLE

Electric Potential patterns Deduced for the SUNDIAL Period of September 23-26, 1986

5. FUNDING NUMBERS

61102F 2310 A2

6. AUTHOR(S)

See Back

7. PERFORMING ORGANIZATION NAME(S) AND ADDRESS(ES)

SRI International
333 Ravenswood Avenue
Menlo Park, CA 94025-3493

8. PERFORMING ORGANIZATION REPORT NUMBER

AFOSR-TR 91 0466

9. SPONSORING / MONITORING AGENCY NAME(S) AND ADDRESS(ES)

AFOSR/NC
Building 410, Bolling AFB DC
20332-6448

10. SPONSORING / MONITORING AGENCY REPORT NUMBER

F49620-87-K-0007

11. SUPPLEMENTARY NOTES

Annales Geophysicae, 1990, 8, (6), 399-408

12a. DISTRIBUTION / AVAILABILITY STATEMENT

APPROVED FOR PUBLIC RELEASE; DISTRIBUTION IS UNLIMITED

12b. DISTRIBUTION CODE

13. ABSTRACT (Maximum 200 words)

ABSTRACT High-latitude electric potential and ionospheric conductance patterns are presented and discussed for the Northern Hemisphere during the SUNDIAL period of September 23-26, 1986 using the Assimilative Mapping of Ionospheric Electrodynamics (AMIE) technique of Richmond and Kamide (1988). Data sources used for the model are satellite and ground magnetometers, electron precipitation instruments, incoherent scatter radars, and ionospheric coherent radars. The period was characterized by many substorms, and a wide variety of instantaneous patterns of electrodynamic parameters on a hemispheric scale are derived throughout this period, of which only a few examples are displayed. The entire set of electric potentials and conductances are being made available through the NCAR CEDAR Data Base for further analysis and utilization in simulation models.

14. SUBJECT TERMS

15. NUMBER OF PAGES
10

16. PRICE CODE

17. SECURITY CLASSIFICATION OF REPORT	18. SECURITY CLASSIFICATION OF THIS PAGE	19. SECURITY CLASSIFICATION OF ABSTRACT	20. LIMITATION OF ABSTRACT
UNCLASSIFIED	UNCLASSIFIED	UNCLASSIFIED	SAR

Electric potential patterns deduced for the SUNDIAL period of September 23-26, 1986

B. A. EMERY (1), A. D. RICHMOND (1), H. W. KROEHL (2), C. D. WELLS (2), J. M. RUOHONIEMI (3), M. LESTER (4), D. J. KNIPP (5), F. J. RICH (6), J. C. FOSTER (7), O. DE LA BEAUJARDIÈRE (8), C. SENIOR (9), L. M. SHIER (1), J. F. McKEE (2), and S. MAEDA (10)

(1) *High Altitude Observatory, National Center for Atmospheric Research, P.O. Box 3000, Boulder, CO 80307, USA*
(2) *National Geophysical Data Center, NOAA, 325 Broadway, Boulder, CO 80303, USA*
(3) *Applied Physics Laboratory, Johns Hopkins University, Johns Hopkins Road, Laurel, MD 20707, USA*
(4) *Department of Physics, University of Leicester, University Road, Leicester LE1 7RH, UK*
(5) *Physics Department, US Air Force Academy, Colorado Springs, CO 80840, USA*
(6) *Geophysics Laboratory, Hanscom Air Force Base, Bedford, MA 01731-5000, USA*
(7) *MIT Haystack Observatory, Westford, MA 01886, USA*
(8) *Stanford Research Institute International, 333 Ravenswood Avenue, Menlo Park, CA 94025, USA*
(9) *Centre de Recherche en Physique de l'Environnement, 4 avenue de Neptune, 94107 Saint-Maur des Fossés, France*
(10) *Osaka College, Hirao, Mihara, Minamikawachi, Osaka 587, Japan*

Received October 3, 1989; revised January 25, 1990; accepted January 26, 1990.

ABSTRACT. High-latitude electric potential and ionospheric conductance patterns are presented and discussed for the Northern Hemisphere during the SUNDIAL period of September 23-26, 1986 using the Assimilative Mapping of Ionospheric Electrodynamics (AMIE) technique of Richmond and Kamide (1988). Data sources used for the model are satellite and ground magnetometers, electron precipitation instruments, incoherent scatter radars, and ionospheric coherent radars. The period was characterized by many substorms, and a wide variety of instantaneous patterns of electrodynamic parameters on a hemispheric scale are derived throughout this period, of which only a few examples are displayed. The entire set of electric potentials and conductances are being made available through the NCAR CEDAR Data Base for further analysis and utilization in simulation models.

Annales Geophysicae, 1990, **8**, (6), 399-408.

1. INTRODUCTION

The high-latitude distribution of ionospheric electric potential is a sensitive indicator of the coupling between the solar wind, the interplanetary magnetic field (IMF) and the magnetosphere/ionosphere. It is also an important input to simulation models of ionospheric and thermospheric dynamics (e.g. Crowley *et al.*, 1989*a*, *b*; Rasmussen *et al.*, 1986). We have inferred the patterns of convection and ionospheric conductance every 10 min during the joint SUNDIAL/GISMOS period of September 23-26, 1986 using measurements from ground and satellite-based magnetometers, coherent and incoherent scatter radars, and satellite electron electrostatic analyzers in the Assimilative Mapping of Ionospheric Electrodynamics (AMIE) procedure of Richmond and Kamide (1988). This method yields the distribution of the electrostatic potential over the northern polar region. The computed potentials are derived self-consistently from different measurements of diverse electrodynamic parameters and provide the best estimates of the large-scale instantaneous patterns.

The AMIE technique is described in detail in Richmond and Kamide (1988), and has been previously applied to three other campaign periods. These are: the GISMOS (Global Ionospheric Simultaneous Measurements Of Substorms) period of January 18-19, 1984 (Richmond *et al.*, 1988, 1990; Knipp, 1989), the ETS (Equinox Transition Study) period of September 19, 1984 (Knipp *et al.*, 1989; Knipp, 1989), and the period of July 23-24, 1983 (Knipp, 1989). These studies showed that realistic electric potential patterns could be derived. In regions where the inferred electric fields depend primarily on ground magnetometer data, the largest uncertainties were in the specification of the ionospheric conductance. These uncertainties can be reduced by the inclusion of spacecraft electron precipitation measurements (Knipp *et al.*, 1989; Knipp, 1989).

The purpose of the present paper is to describe concisely the types of data utilized to obtain the

convection patterns for this SUNDIAL period of study, to present a few examples of patterns displaying noteworthy characteristics, and to summarize the general behaviour of high-latitude electrodynamic activity for the days of September 23-26, 1986. Because of potential interest in further utilization and analysis of the time-varying convection patterns, we are making them available now in digital form to the scientific community, even though our own analysis of them has only begun.

2. GEOPHYSICAL CONDITIONS

The SUNDIAL period of September 22-26, 1986 is representative of solar minimum conditions. The daily 10.7 cm solar flux varied between 68.3 and 69.4 during this period. The K_p was low (2 + or less) on September 22, and then varied between 6 and 2 on September 23-26, with the lowest values during the first part of September 25 and the latter part of September 26. This variety of conditions is reinforced in Figure 1*a*, which shows hourly averages of the interplanetary magnetic field north-south component (IMF B_z) for this period. Lower values of K_p are generally associated with positive IMF B_z. The quiet day of September 22, 1986 was used as the baseline from which to measure the ground magnetic variations on September 23-26, 1986. Figure 1*b* shows hourly averages of the IMF B_y. September 23-26, 1986, was generally a period of IMF B_y negative (and B_y positive). The *AE* index was computed using extreme variations in the magnetic north component from the

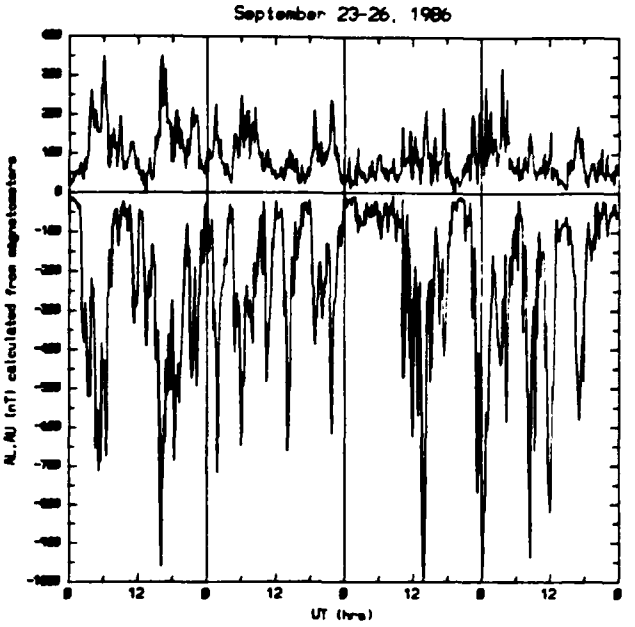

Figure 2
The AL and AU calculated every 10 min *from the* 19 *ground magnetometer stations between* 55 and 76° *for the* AMIE *study for September* 23-26, 1986.

19 ground magnetometer stations used in the study which were located between 55 and 76 degrees magnetic north. The resulting *AL* and *AU* indices computed every 10 min are shown in Figure 2. The *AL* index in particular is very active in this period, indicating the presence of many substorms.

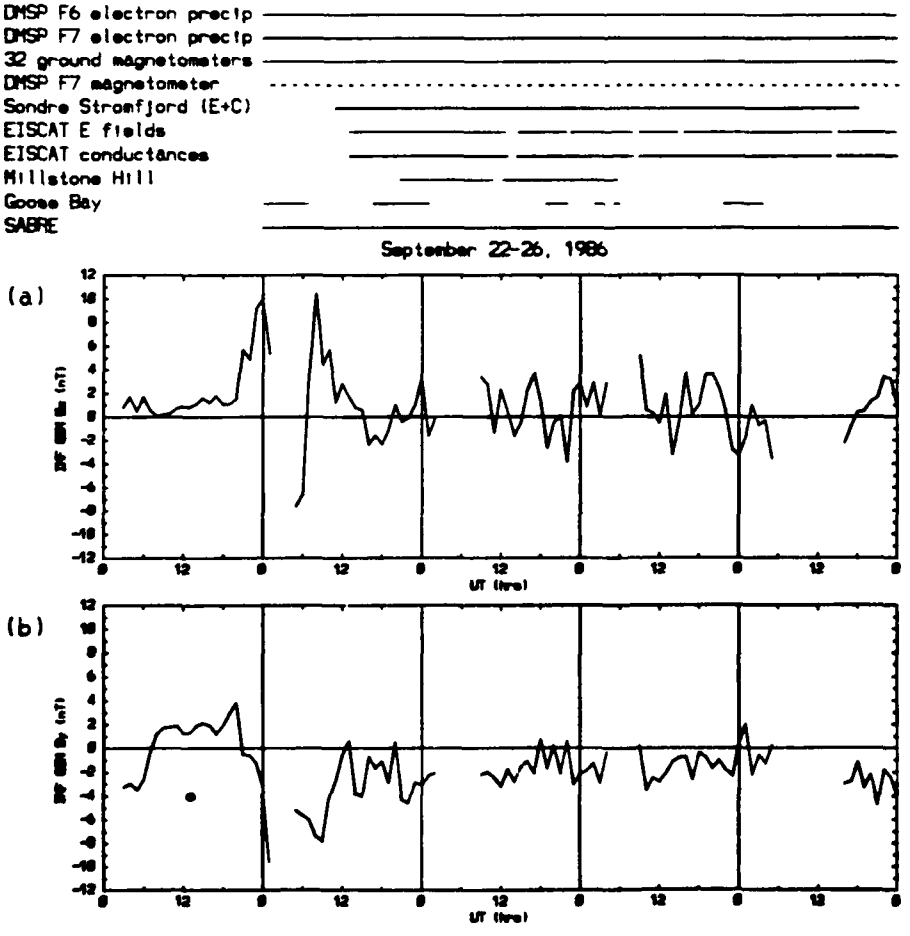

Figure 1
Hourly IMF (a) B_z *and* (b) B_y *values on September* 22-26, 1986 *and the times of data coverage for the various data sources used in the* AMIE *run for September* 23-26, 1986.

3. STATISTICAL INPUTS

The AMIE technique starts from statistical models of auroral conductances and electric potential, and modifies these in accordance with the actual measurements for the time of interest. The statistical models not only provide a hemispheric distribution, but also provide a reasonable reference in regions where no observations are available.

For the present study, we use the statistical auroral conductance model of Fuller-Rowell and Evans (1987), which is parameterized by the 10-level hemispheric power index defined in Foster *et al.* (1986*b*). This index is normally derived from electron precipitation measurements on board the NOAA series of satellites, but instrumental problems made these data unusable for most of our SUNDIAL period (Evans, private communication). Consequently, we estimated the appropriate power level from an empirical relationship with hourly values of the hemispheric power and the *AE* index, where

$$P(\mathrm{GW}) = 4.28 + 0.0624 \cdot AE\,(\mathrm{nT})\,.$$

The correlation coefficient for this relationship is 0.71. We used this formula with instantaneous *AE* values where we subtracted 25 nT to account for the larger number of stations used in our index compared to the regular index (Kroehl, 1989). This relationship is analogous to the relation of power to K_p published by Maeda *et al.* (1989).

Observations are used to modify the statistical auroral conductance patterns, which are combined with an empirical model of conductance produced by solar ultraviolet radiation to yield the total conductance. This model of solar ultraviolet produced conductances is a new one that includes the 10.7 cm solar flux variations as well as season, time of day, and magnetic latitude. This model is based on Chatanika radar observations of electron densities (Kroehl *et al.*, manuscript in preparation). Since the September 1986 period of interest was near the minimum of the solar cycle, it is important to have the conductance model reflect solar minimum conditions, especially in the polar cap.

Most previous studies using the AMIE technique utilized the statistical electric potential model of Foster *et al.* (1986*b*), which is also based on the 10-level hemispheric power index, and was derived from seven years of Millstone Hill radar measurements. In a later study, Foster (1987) combined Søndre Strømfjord and Millstone Hill radar ion drifts to produce global electric potential patterns as a function of IMF B_y and B_z. For the present study, the initial electric potential patterns in AMIE use the four statistical patterns of Foster (1987) if both IMF component magnitudes interpolated from hourly values are greater than 0.5 nT. For smaller magnitudes, the statistical patterns based on the hemispheric power level (Foster *et al.*, 1986*b*) provide the initial electric potential. The parameterization of the statistical electric potential by IMF B_y and B_z is new to the AMIE procedure, and was chosen because the polar cap region is not well specified by data during this period. When the polar cap is in darkness, and the conductivities are small, the ground magnetometers cannot easily sense the effects of the electric fields present there. We discuss briefly in Section 5 the sensitivity of the results to the choice of statistical models.

4. DATA INPUTS

The data sources that were incorporated into the electric potential pattern determination included both ground and satellite observations. There were 32 ground magnetometer stations, which are listed in Table 1. The other sources are listed in Table 2 and include three incoherent scatter radars, two ionospheric coherent radars, one satellite magnetometer and particle precipitation instruments on two satellites. The time coverage of these data sources are shown in Figure 1 above the plot of B_z. Data that covered an extended latitude range were averaged over about 2.5° of magnetic latitude in order to be compatible with the spatial resolution employed here in the AMIE procedure.

Table 1

Ground Magnetometer Stations

These stations were used in the AMIE procedure in the SUNDIAL campaign period of September 23-26, 1986. September 22, 1986 was used as the quiet day from which differences were found for the disturbed days.
(D) = needed to be digitized
(*) = provided conductance with formulas modified from Ahn *et al.* (1983).

Station	Mag Lat	Mag Lon
Resolute Bay, Canada	84.1	304.3
Mould Bay, Canada	80.6	263.5
Cambridge Bay, Canada	77.8	299.7
New Aalesund, Norway (D)	75.9	114.7
Baker Lake, Canada	75.2	320.0
*Cape Chelyuskin, USSR (D)	71.6	174.2
*Fort Churchill, Canada	70.3	326.0
*Barrow, USA	69.7	248.1
*Yellowknife, Canada	69.6	294.4
*Narssarssuaq, Greenland	68.9	44.0
*Dixon Island, USSR (D)	68.3	154.7
*Poste-de-la-Baleine, Canada	68.0	353.8
*Leirvogur, Iceland (D)	66.8	69.6
*Tixie Bay, USSR (D)	65.8	195.5
*College, USA	64.8	259.6
*Meanook, Canada	62.6	300.9
*Cape Wellen, USSR (D)	62.5	242.6
*Glenlea, Canada	60.4	326.8
Sitka, USA	59.8	277.8
Ottawa, Canada	58.5	356.2
Saint Johns, Canada	57.6	29.1
Point Tunguska, USSR (D)	56.5	162.5
Victoria, Canada	54.1	292.4
Magadan, USSR (D)	53.9	217.4
Borok, USSR (D)	53.6	114.2
Sverdlovsk, USSR (D)	52.7	132.5
Fredericksburg, USA	50.2	355.6
Valentia, Ireland (D)	50.1	71.8
Boulder, USA	49.5	315.7
Irkutsk, USSR (D)	46.6	176.4
Bay Saint Louis, USA	41.8	338.5
Memambetsu, Japan	37.4	213.7

Table 2
Radars and Satellites

These instruments were used in the AMIE procedure in the SUNDIAL campaign period of September 23-26, 1986.

Instrument	Range in Magnetic Coordinates
Søndre Strømfjord, Greenland	68 to 80 N, 42.7 E
EISCAT	62 to 72 N, 104.7 E
Millstone Hill, USA	50 to 70 N, -15 to 30 E
Goose Bay, Canada	65 to 77 N, 22.0 E
SABRE	62 to 65 N, 91.3 E
DMSP F7 magnetometer	50 to 90 N, near 10:30-22:30 MLT
DMSP F6 electron detector	50 to 90 N, near 6:00-18:00 MLT
DMSP F7 electron detector	50 to 90 N, near 10:30-22:30 MLT

4.*a*) Ground magnetometers

All three components of the measured magnetic perturbation at the ground are utilized in this study, including the vertical component. Knipp (1989) has detailed how these perturbations are utilized within the AMIE procedure. The magnetic perturbations are used primarily to determine the ionospheric electric field and current patterns, but also used to modify the auroral conductance model, as described by Richmond and Kamide (1988) and Richmond *et al.* (1988) based on a modified form of empirical relations presented by Ahn *et al.* (1983). The instantaneous values of the magnetometer data were used in the study without averaging since the variations were relatively smooth in time.

4.*b*) Incoherent scatter radars

All of the incoherent scatter radars which operate in the high-latitude Northern Hemisphere were operating in the SUNDIAL 1986 period. Figure 1 shows that Søndre Strømfjord and EISCAT started at 1100 and 1300 UT, respectively, on September 23, 1986, after the second excursion of B_z to large positive values. The two radars continued to operate until 1810 and 2350 UT, respectively, on September 26, 1986. The Millstone Hill radar operated from 2040 UT on the 23rd to 0530 UT on the 25th.

The Søndre Strømfjord radar scanned in geomagnetic latitude every 18 min and provided ion velocities perpendicular to the field which were averaged in bins of 2.4° of apex latitude. The EISCAT radar was operated in the CP-3-E mode which had a scan cycle of 30 min. The bisector measurements were converted to perpendicular and parallel components and averaged in 2.3° latitude bins. Millstone Hill operated with alternate low-elevation azimuth scans from the east to the north-west, and magnetic-meridian elevation scans over a period of 24 min. The former were used to obtain binned line-of-sight velocities approximately perpendicular to the geomagnetic field. For all of the radars, all data within the period of one complete scan centered around the time of calculation were accepted by the AMIE procedure, though the errors assigned to the data were increased for the data that were not close to the time of calculation. The Søndre Strømfjord and EISCAT radars also provided near-overhead ionospheric conductance measurements that were used to help determine the auroral conductance distributions.

4.*c*) Ionospheric coherent radars

The SABRE (Sweden and Britain Radar Experiment) VHF coherent scatter radar provided *E* region electron drift estimates (Nielsen *et al.*, 1983). The data were separated into two latitude regions between 62 and 65° magnetic latitude and averaged over 5 min intervals over the entire longitude viewing area before being converted to electric field values. Since the velocity measurements saturate at the phase velocity of the *E*-region irregularities, these electric fields may be lower limits on the actual values. The data were available on a continuous basis, with small signal return indicating small electric fields, typically less than 10 to 15 mV/m. Data within ± 5 min of the calculation time were included, with larger error bars for data 5 min away.

The Goose Bay HF coherent scatter radar (Greenwald *et al.*, 1985) provides *F* region irregularity drifts, which are similar to the *F* region ion drifts (Ruohoniemi *et al.*, 1987). A lack of return signal does not indicate small ion velocities, but only the absence of strong irregularities. There were several data dropouts in the time period as shown in Figure 1. The data were averaged every 10 min over 2° bins in magnetic latitude and over the entire longitude viewing area before being converted to electric fields. The scanning region covered between 65 and 77° magnetic latitude for this period, but more commonly only provided one or two positions in magnetic latitude. All data within 15 min of the calculation time were used. This is the first time these data have been included in the AMIE procedure.

4.*d*) DMSP F7 magnetometer

The DMSP F7 satellite contained a magnetometer that was flown in approximately the pre-noon, pre-midnight region over the pole (Rich and Gussenhoven, 1987). As described by Knipp (1989), the gradient of the horizontal magnetic perturbations along the satellite track was derived and averaged over 40 s intervals (about 300 km in distance) and used to determine the large-scale field-aligned current structure. The gradient rather than the magnetic perturbation itself was used in order to minimize the influence of residual undetermined crustal geomagnetic fields as well as the effects of large-scale ionospheric currents, both of which have relatively small gradients at satellite altitudes in comparison with the effects of local field-aligned currents. Any data within 20 min of the calculation time were included in the AMIE procedure, but with larger errors assigned to the temporally more distant data.

4.*e*) DMSP F6 and F7 precipitating electron data

Rich *et al.* (1987) describe how auroral conductance enhancements can be derived from the DMSP electrostatic analyzers using the formulas of Robinson *et al.* (1987). We use 40 s averages obtained from the F6

and F7 satellites, which are in sun-synchronous orbits with approximate equatorial crossings at dawn and dusk (F6) and at 10 : 30 LT and 22 : 30 LT (F7). We included Southern Hemisphere data mapped to Northern geomagnetic conjugate locations on the supposition that conjugacy of precipitation is valid on the 300 km spatial scale we employ (see Mizera *et al.*, 1987). However, the Southern Hemisphere measurements are assigned a 50 % larger error to account for imperfect conjugacy.

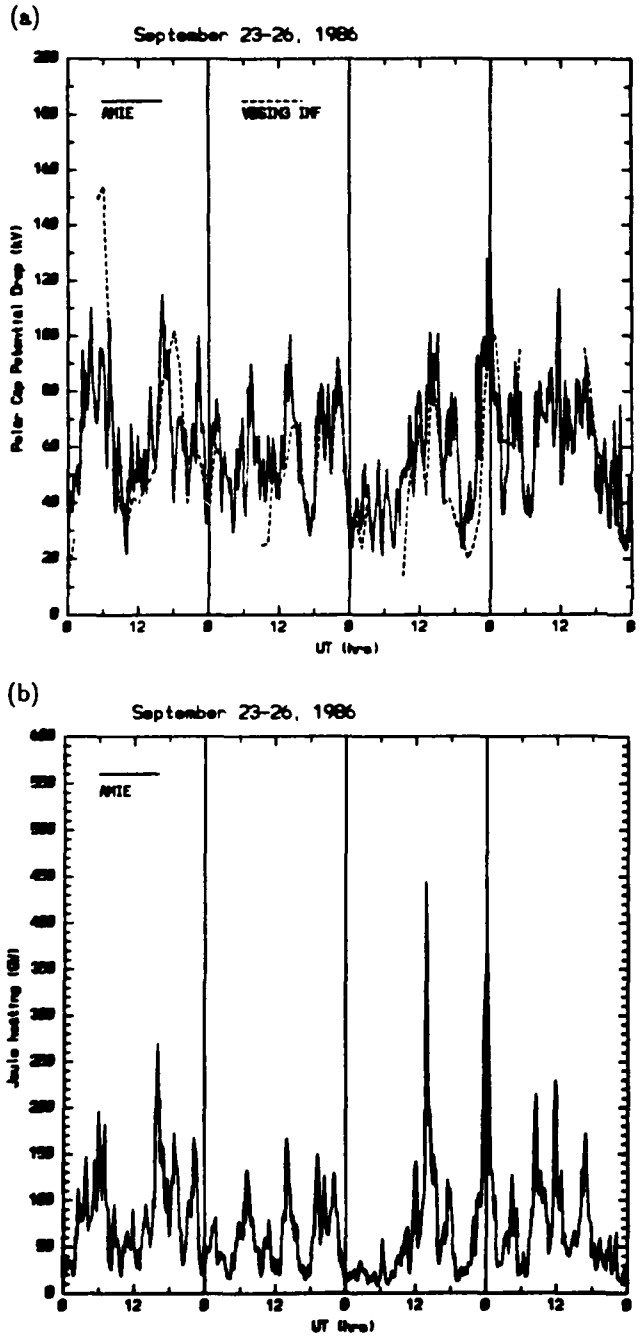

Figure 3

(a) *The polar cap potential drop calculated every* 10 min *from the* AMIE *study of September* 23-26, 1986. *Also plotted are the potential drops derived using the* $vB\sin^3(\Theta/2)$ *formula involving the* IMF B_z, B, *and the solar wind speed* v *(Reiff and Luhmann,* 1986). (b) *The accompaning Joule heating derived from the Pedersen conductance and the electric field, corrected for expected additional magnitudes. Neutral winds are assumed to be zero.*

5. RESULTS

Figure 3*a* is a plot of the polar cap potential difference for September 23-26, 1986 derived from the AMIE technique and the $vB\sin^3(\Theta/2)$ formula of Reiff and Luhmann (1986) using hourly averages of IMF and solar wind data. Here, v is the solar wind speed in km/s, B is the GSM IMF, maximized at 9 nT, and $\Theta = \arccos(B_z/B)$. The potential from the IMF formula is composed of 57 % of the potential from the present hour, 29 % of the potential from the past hour, and 14 % of the potential from the hour before that to allow the ionosphere to remember past conditions (Reiff, private communication). The correspondence between the AMIE potentials and the IMF potentials is quite good for this campaign, with the larger disagreements occurring after IMF data gaps. The polar cap potential drop is anti-correlated with the IMF B_z, and shows rapid fluctuations between 20 and 110 kV, with a maximum potential drop of 127.9 kV occurring at 2330 UT on September 25, 1986. Figure 3*b* is the corresponding plot of the Joule heating derived from the Pedersen conductance and the electric field. Included in the total Joule heating is the correction to the electric field magnitude associated with uncertainties in the electric field, as explained by Richmond *et al.* (1990). A maximum value of 443.8 GW is found at 1340 UT on September 25, 1986, which can be compared to a derived hemispheric power input of 61.0 GW.

Figures 4*a* through 4*d* show the electric potential and the electric and magnetic data on September 24 at 0030 UT and 0100 UT when numerous radar electric field data defined the night side potential values. All five radars were operating during these times (M = Millstone Hill, G = Goose Bay, S = Søndre Strømfjord, A = SABRE, and E = EISCAT), and help produce a distinct change in the character of the potential pattern near midnight between 0030 and 0100 UT. Such coverage can be useful for local studies of substorms or other phenomena.

There are indications that the convection pattern undergoes major global changes at times, in addition to the regional changes shown in Figure 4. Figure 5 shows an event where the two-cell convection appears to be distorted by a general clockwise rotation and a strong intensification of the positive potential cell at 1400 UT on September 25, 1986. Figures 2 and 3 show this to be just after a time when the *AL* index, the polar cap potential drop, and the Joule heating have among the most extreme values for the entire period. In particular, the *AL* index has been less than − 100 nT for three hours, and is now − 860 nT. This value comes from a station in the midnight sector, indicating the presence of strong westward currents associated with the substorm expansion current system (Kroehl and Kamide, 1985). The 1 min IMF B_z values are generally negative around this time, with only 2 brief excursions to positive values around 1320 and 1345 UT. The 1 min B_z values have been negative for just over 1 h.

In Figure 5*a*, the negative cell in the afternoon is fairly well defined by the radar measurements for this case,

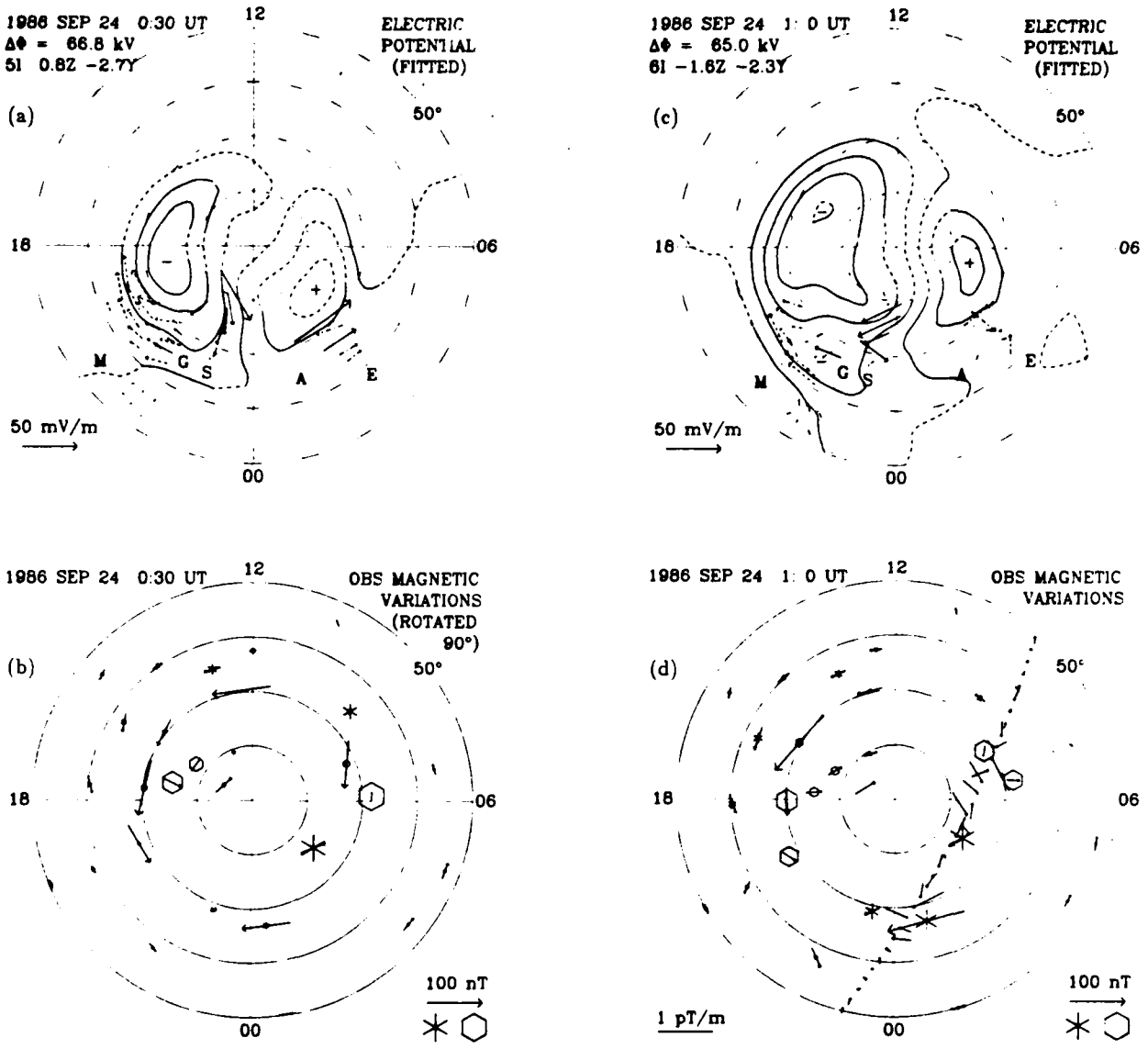

Figure 4

(a) *Electric potential derived for* 0030 UT *on September* 24, 1986, *with superposed electric field observations, which have been rotated* 90° *counterclockwise to show the direction of plasma flow. Contours are spaced at* 10 kV, *and are dashed in regions where the* AMIE *procedure infers an uncertainty in the large scale electric field greater than* 50 %, *not including the effects of uncertainties in the conductance. The letters* M, G, S, A, *and* E *indicate the observations obtained by the Millstone Hill, Goose Bay, Søndre Strømfjord, SABRE and EISCAT radars, respectively. The Millstone Hill vectors are dashed to indicate that only the line-of-sight velocity component was used as input data, with the transverse component being derived from the* AMIE *fit. Vectors in the long-short dash pattern have large error bars compared to other vectors. At the upper left are given the total potential drop* $\Delta\Phi$, *the initial hemispheric power level I, and the* IMF B_z *and* B_y *values in nanotesla interpolated from hourly values.* (b) *The ground magnetic perturbations used to help determine the electric potential shown in* (a). *Magnetic stations located below* 50° *are not plotted, but are included in the calculations. The horizontal perturbations are rotated* 90° *clockwise to indicate the direction of overhead equivalent current, while the vertical perturbations are shown by stars (downward) or hexagons (upward).* (c) *As in* (a), *but for* 0100 UT. (d) *As in* (b), *but for* 0100 UT, *and with the addition of* DMSP F7 *magnetic perturbation gradients along the satellite track, which passes from the top toward the bottom. Perturbations lying on the dawn side of the track are associated with upward field-aligned currents while perturbations towards the dusk side are associated with downward field-aligned currents. A scale of* 1 pT,m *is given at the lower left for these perturbations.*

whereas the positive cell is determined primarily by the ground and satellite magnetometer data. Since the inference of electric fields from the magnetometer data is sensitive to the conductance model, which has its own uncertainties, the characteristics of the positive potential cell in Figure 5*a* are less reliable than those of the negative cell. Fortunately, the coverage of conductance data for this particular time was relatively extensive owing to the DMSP F6 and F7 overflights. Figure 5*d* shows the auroral Hall conductances inferred from these satellite data, along with total (auroral and solar ultraviolet) conductances measured at Søndre Strømfjord and inferred from ground magnetometers, superposed on the fitted distribution of Hall conductances determined by AMIE. For comparison the unmodified statistical conductance model for this time is shown in Figure 5*c*. As is typically found, the observations tend to make the region of enhanced auroral conductances in Figure 5*d* narrower, with greater peak values, than given by the statistical model in Figure 5*c*. However, the hemispheric power deduced from the fitted conductance and associated auroral energy flux patterns is somewhat reduced, leading to a lower power level.

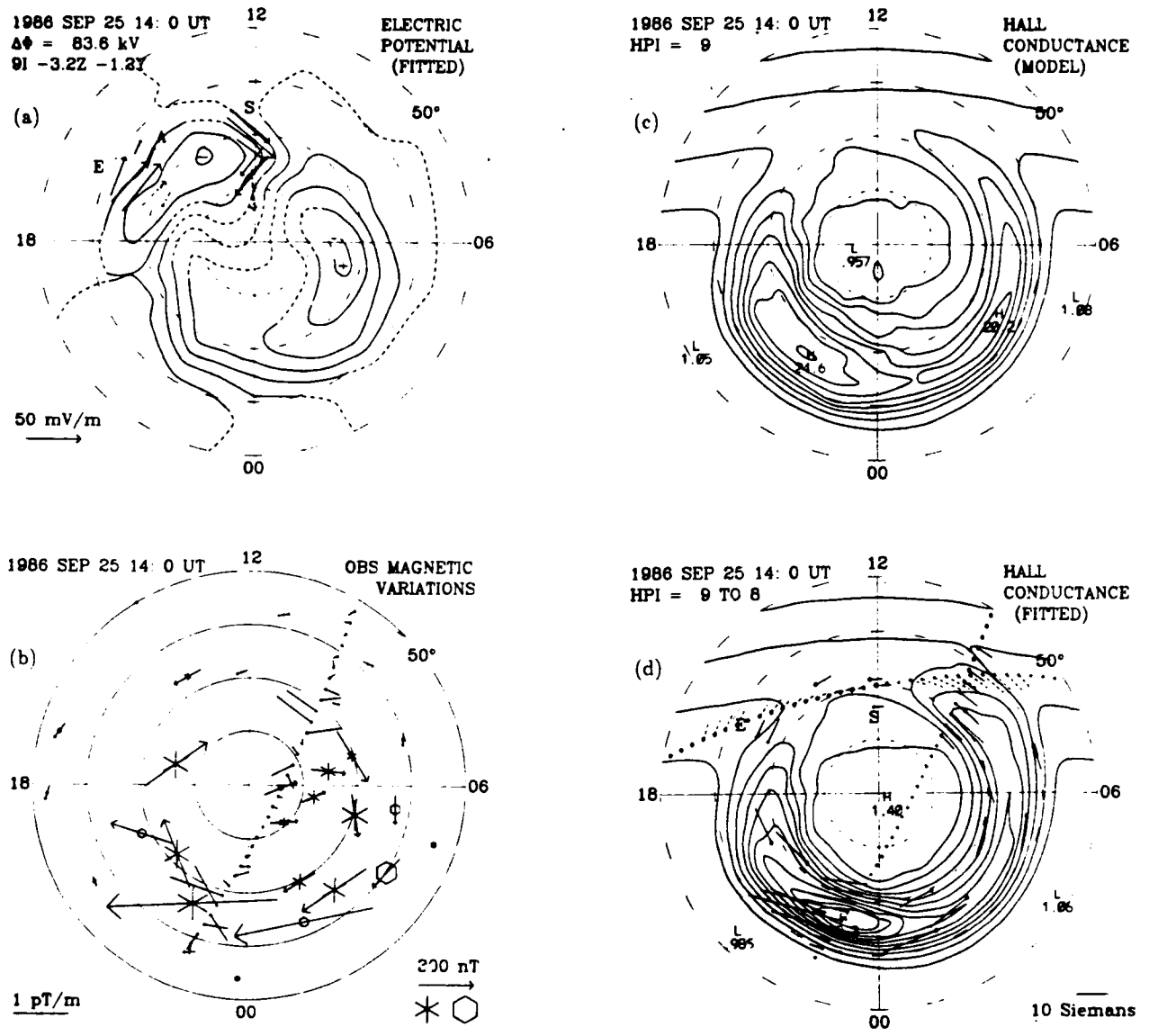

Figure 5

(a) *As in Figure 4a, but for* 1400 UT *on September* 25, 1986. (b) *As in Figure 4d, but for* 1400 UT *on September* 25, 1986. *Note the change in scale of the ground magnetic perturbations.* (c) *Statistical model of Hall conductance obtained by combining the auroral model of Fuller-Rowell and Evans* (1987) *for a hemispheric power index of* 9 *with a solar ultraviolet conductance model appropriate to* 1400 UT *on September* 25, 1986. *Contour intervals are* 3 *Siemens.* (d) *Hall modified conductance, with superposed data, for* 1400 UT *on September* 25, 1986. *Contour intervals are* 3 *Siemens. The observations are indicated by a vector extending towards the west of the observing location, with a scale shown at the lower right of the figure. Thirteen ground magnetometer stations contribute total (auroral combined with solar ultraviolet) conductance measurements in the auroral zone. The letters « S » and « E » show the locations of the Søndre Strømfjord and* EISCAT *measurements of the total conductance.* DMSP F7 *auroral conductances inferred from Northern Hemisphere electron precipitation measurements are shown by solid vectors where a « o » indicates a satellite time before the calculation and a « + » indicates a satellite time afterwards.* DMSP F6 *auroral conductances inferred from Southern Hemisphere data under the assumptions of conjugacy are shown by dashed vectors. The estimated hemispheric power index at this time was* 8, *reduced from the initial level of* 9 *by the measurements.*

Figures 5*e* and 5*f* are plots of the total horizontal and field-aligned currents for this time. The eastward auroral electrojet in the afternoon is associated with the negative electrostatic potential cell. The westward electrojet in the morning and premidnight sectors is associated with the positive cell which is strongly distorted from a symmetric convection-driven distribution on the nightside by auroral substorm processes (Kroehl and Kamide, 1985). The field-aligned currents in Figure 5*f* display well-defined Region *I* and Region *II* current systems (Iijima and Potemra, 1978), where Region *I* is the downward current near 0600 LT and the upward current near 1800 LT. The gradient in the magnetic perturbation field measured by the DMSP F7 magnetometer is superposed on the field-aligned current distribution. Since the satellite was traveling from the dayside to the nightside, the along-track magnetic perturbation gradients tend to be associated with downward field-aligned currents when the plotted vector is directed toward the dusk side of the track, and upward currents when the vector is toward the dawn side. Upward currents are usually associated with the more intense areas of particle precipitation. The extension of the westward electrojet and the associated downward field-aligned currents past the dusk meridian is also found in the study of Kamide *et al.* (1982), and appears to be related to a later phase in substorm processes. The distorted morning cell and

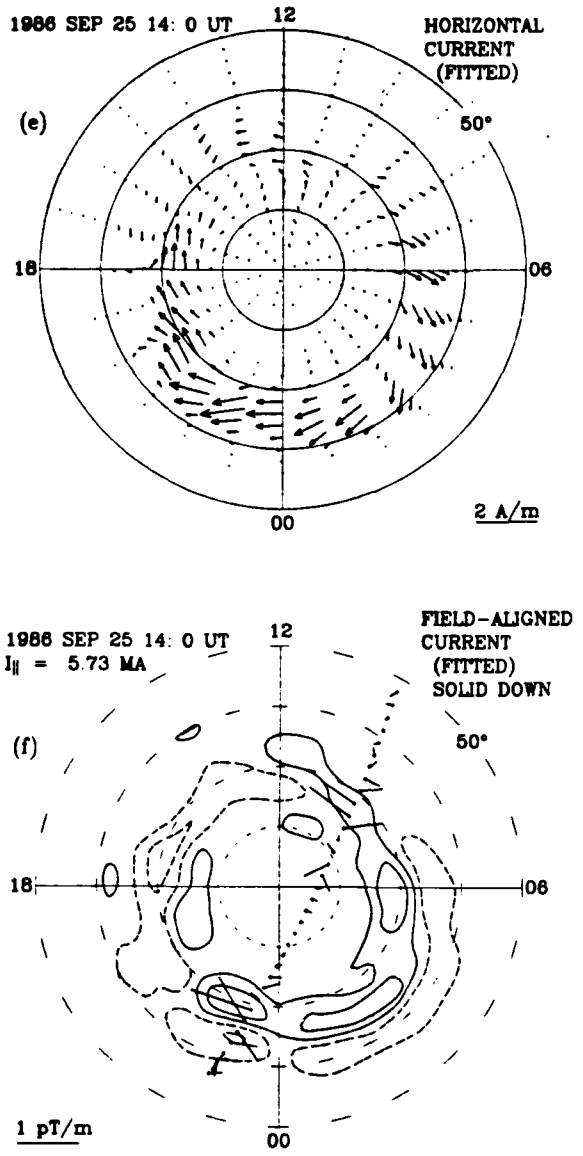

Figure 5e, f

(e) *Height-integrated horizontal ionospheric current for* 1400 UT *on September* 25, 1986, *where a vector of length equal to* 10° *in latitude corresponds to* 2 A m. (f) *Field-aligned current density derived for* 1400 UT *on September* 25, 1986. *Solid contours represented downward current. The contour interval is* 0.5 μA m^{-2} *starting at* $\pm$ 0.25 μA m^{-2}. *The* DMSP F7 *magnetometer perturbations, as described in Figure 4d, are superposed.*

associated westward substorm expansion current in the midnight sector recurs several times in the four day period, usually near or just following peaks in the *AL* (or *AE*) index.

In general, the convection for this 4-day period often tended to have features commonly associated with convection under negative IMF B_y conditions, namely, an expanded dawn convection cell, a stronger convection reversal shear in the dusk cell, and a northeastward flow in the dayside throat region (de la Beaujardière *et al.*, 1986; Foster *et al.*, 1986*a*; Heppner and Maynard, 1987). Figure 5*a* is one example of this, although it also displays the additional substorm features on the nightside mentioned above. During periods when the IMF B_y was positive, the dusk cell usually expanded relative to the dawn cell, again in general accord with previous statistical analyses.

We carried out several sensitivity studies to test the stability and robustness of the derived patterns of electric potential, current, and Joule heating to changes in the initial statistical potential model employed and to deletions of various subsets of the data. As expected on the basis of previous tests (Richmond *et al.*, 1988; Knipp, 1989), noticeable changes in the patterns follow from changes in the inputs to the AMIE procedure, but most of the global characteristics tend to be preserved among the various tests. The use of an IMF-parameterized statistical potential (Foster, 1987) in place of one not based on the IMF (Foster *et al.*, 1986*b*) changed the shape of the electric potential contours in the polar cap, particularly when direct electric field observations in the polar cap were missing. We plan to present in more detail the results of the sensitivity studies in a future publication.

6. SUMMARY

The synthesis of several diverse data sets relating to high-latitude electric fields and currents has enabled us to obtain an approximate picture of the time-varying convection patterns in the Northern polar region for September 23-26, 1986. The ability to include coherent scatter as well as incoherent scatter radar data has improved the ability to define the convection in certain regions and for longer periods, while the inclusion of the three-component ground magnetometer data and horizontal satellite magnetometer data has also helped to constrain the derived patterns. Other significant improvements we have introduced include the utilization of an IMF B_y and B_z dependent statistical electric potential model as a point of departure, and a solar cycle dependent model of the solar ultraviolet component of ionospheric conductance.

The period September 23-26, 1986 contained considerable substorm activity. During the later phase of the substorms, the dawn convection cell often expanded into the pre-midnight region in conjunction with the westward electrojet. IMF B_y-dependent features in the relative sizes and orientations of the dawn and dusk convection cells were often apparent, that generally agreed with features deduced statistically in previous studies.

The electric potentials and conductances should be useful for further modeling studies, and are being made available through the NCAR CEDAR Data Base in digital form every 10 min from September 23 at 0000 UT to September 26 at 2350 UT on a grid of the Northern Hemisphere above 50° apex latitude. The grid spacing is every 2° from 50 to 90 and every hour of magnetic local time.

Acknowledgements

The incoherent scatter radar data for September 23-26, 1986 were taken from the NCAR CEDAR Data Base (formerly the NCAR Incoherent Scatter Radar

Data Base). The CEDAR Data Base, along with the Millstone Hill and Søndre Strømfjord radars, is supported by the National Science Foundation. The EISCAT Scientific Association is supported by Centre National de la Recherche Scientifique of France, Suomen Akatemia of Finland, Max-Planck-Gesellschaft of Germany, Norges Almenvitenskapelige Forskningsråd of Norway, Naturvetenskapliga Forskningsrådet of Sweden, and the Science and Engineering Research Council of the United Kingdom. SABRE is a joint project between the University of Leicester in Leicester, United Kingdom, the Max Planck Institute for Aeronomy in Lindau, West Germany, and the Uppsala Ionospheric Observatory in Uppsala, Sweden. Goose Bay is supported in part by the National Science Foundation and the Air Force Office of Scientific Research. The Geophysics Laboratory is partly responsible for the operations at the Goose Bay site. The IMF hourly data were taken from files kept by the National Space Science Data Center (NSSDC) of the National Aeronautics and Space Administration (NASA). Plots of the 1 minute IMF data were provided courtesy of Dr. R. Lepping of the NASA Goddard Space Flight Center and are also available in digital form through the NSSDC. The DMSP precipitating electron data were processed by K. Lutz at the National Geophysical Data Center. S. Maeda is grateful to the Cooperative Institute for Research in the Environmental Sciences at the University of Colorado for assistance in her stay at the NOAA Space Environment Laboratory. We would like to acknowledge the following grants: NASA contract W-16320, NSF grant ATM-87-13982, SERC grant GR/E 73963, AFOSR task number 2311G5, NSF Cooperative Agreement ATM 88-08137, and AFOSR contract F49620-87-K-007.

REFERENCES

Ahn, B.-H., S.-I. Akasofu, and Y. Kamide, The Joule heat production rate and the particle energy injection rate as a function of the geomagnetic indices *AE* and *AL*, *J. Geophys. Res.*, **88**, 6275-6287, 1983.

Crowley, G., B. A. Emery, R. G. Roble, H. C. Carlson, and D. J. Knipp, Thermospheric dynamics during September 18-19, 1984: 1. Model simulations, *J. Geophys. Res.*, **94**, 16925-16944, 1989*a*.

Crowley, G., B. A. Emery, R. G. Roble, H. C. Carlson, J. E. Salah, V. B. Wickwar, K. L. Miller, W. L. Oliver, R. G. Burnside, and F. A. Marcos, Thermospheric dynamics during September 18-19, 1984: 2. Validation of the NCAR Thermospheric General Circulation Model, *J. Geophys. Res.*, **94**, 16945-16959, 1989*b*.

de la Beaujardière, O., V. B. Wickwar, and J. H. King, Sondrestrom radar observations of the effect of the IMF B_y component on polar cap convection, in *Solar Wind-Magnetosphere Coupling*, Eds. Y. Kamide and J. A. Slavin, Terra Scientific Publ. Co., 495-505, 1986.

Foster, J. C., Radar-deduced models of the convection electric field, in *Proceedings of the International Symposium on Quantitative Modelling of Magnetosphere-Ionosphere Coupling Processes*, Eds. Y. Kamide and R. A. Wolf, Kyoto, Japan, 71-76, 1987.

Foster, J. C., J. M. Holt, R. G. Musgrove, and D. S. Evans, Solar wind dependencies of high-latitude convection and precipitation, in *Solar Wind-Magnetosphere Coupling*, Eds. Y. Kamide and J. A. Slavin, Terra Scientific Publ. Co., 477-494, 1986*a*.

Foster, J. C., J. M. Holt, R. G. Musgrove, and D. S. Evans, Ionospheric convection associated with discrete levels of particle precipitation, *Geophys. Res. Lett.*, **13**, 656-659, 1986*b*.

Fuller-Rowell, T. J., and D. S. Evans, Height integrated Pedersen and Hall conductivity patterns inferred from the TIROS-NOAA satellite data, *J. Geophys. Res.*, **92**, 7606-7618, 1987.

Greenwald, R. A., K. B. Baker, R. A. Hutchins, and C. Hanuise, An HF phased-array radar for studying small-scale structure in the high-latitude ionosphere, *Radio Sci.*, **20**, 63-79, 1985.

Heppner, J. P., and N. C. Maynard, Empirical high-latitude electric field models, *J. Geophys. Res.*, **92**, 4467-4489, 1987.

Iijima, T., and T. A. Potemra, Large-scale characteristics of field-aligned currents associated with substorms, *J. Geophys. Res.*, **83**, 599-615, 1978.

Kamide, Y., B.-H. Ahn, S.-I. Akasofu, W. Baumjohann, E. Friis-Christensen, H. W. Kroehl, H. Maurer, A. D. Richmond, G. Rostoker, R. W. Spiro, J. K. Walker, and A. N. Zaitzev, Global distribution of ionospheric and field-aligned currents during substorms as determined from six IMS meridian chains of magnetometers: Initial results, *J. Geophys. Res.*, **87**, 8228-8240, 1982.

Knipp, D. J., Quantifying and reducing uncertainty in the Assimilative Mapping of Ionospheric Electrodynamics, PhD thesis in the Department of Atmospheric Science at the University of California in Los Angeles, 1989.

Knipp, D. J., A. D. Richmond, G. Crowley, O. de la Beaujardière, E. Friis-Christensen, D. S. Evans, J. C. Foster, I. W. McCrea, F. J. Rich, and J. A. Waldock, Electrodynamic patterns for September 19, 1984, *J. Geophys. Res.*, **94**, 16913-16923, 1989.

Kroehl, H. W., A critical evaluation of the *AE* indices, *J. Geomagn. Geoelectr.*, **41**, 317-329, 1989.

Kroehl, H. W., and Y. Kamide, High-latitude indices of electric and magnetic variability during the CDAW 6 intervals, *J. Geophys. Res.*, **89**, 1367-1374, 1985.

Maeda, S., T. J. Fuller-Rowell, and D. S. Evans, Zonally averaged dynamical and compositional response of the thermosphere to auroral activity September 18-24, 1984, *J. Geophys. Res.*, **94**, 16869-16883, 1989.

Mizera, P. F., D. J. Gorney, and D. S. Evans, On the conjugacy of the aurora: High and low latitudes, *Geophys. Res. Lett.*, **14**, 190-193, 1987.

Nielsen, E., W. Guttler, E. C. Thomas, C. P. Stewart, T. B. Jones, and A. Hedberg, A new radar auroral backscatter experiment, *Nature*, **304**, 712-714, 1983.

Rasmussen, C. E., R. W. Schunk, and J. J. Sojka, Effects of different convection models upon the high-latitude ionosphere, *J. Geophys. Res.*, **91**, 6999-7005, 1986.

Reiff, P. H., and J. G. Luhmann, Solar wind control of the polar-cap voltage, in *Solar Wind-Magnetosphere Coupling*, Eds. Y. Kamide and J. A. Slavin, Terra Scientific Publ. Co., 453-476, 1986.

Rich, F. J., and M. S. Gussenhoven, The absence of Region 1/Region 2 field-aligned currents during prolonged quiet times, *Geophys. Res. Lett.*, **14**, 689-692, 1987.

Rich, F. J., M. S. Gussenhoven, and M. E. Greenspan, Using simultaneous particle and field observations on a low altitude satellite to estimate Joule heat energy flow into the high latitude ionosphere, *Ann. Geophysicae*, **5**, 527-534, 1987.

Richmond, A. D., and Y. Kamide, Mapping electrodynamic features of the high-latitude ionosphere from localized observations: Technique, *J. Geophys. Res.*, **93**, 5741-5759, 1988.

Richmond, A. D., Y. Kamide, B.-H. Ahn, S.-I. Akasofu, D. Alcaydé, M. Blanc, O. de la Beaujardière, D. S. Evans, J. C. Foster, E. Friis-Christensen, T. J. Fuller-Rowell, J. M. Holt, D. Knipp, H. W. Kroehl, R. P. Lepping, R. J. Pellinen, C. Senior, and A. N. Zaitzev, Mapping electrodynamic features of the high-latitude ionosphere from localized observations: Combined incoherent-

scatter radar and magnetometer measurements for January 18-19, 1984. *J. Geophys. Res.*, **93**, 5760-5776, 1988.

Richmond, A. D., Y. Kamide, S.-I. Akasofu, D. Alcaydé, M. Blanc, O. de la Beaujardière, D. S. Evans, J. C. Foster, E. Friis-Christensen, J. M. Holt, R. J. Pellinen, C. Senior, and A. N. Zaitzev, Global measures of ionospheric electrodynamic activity inferred from combined incoherent-scatter radar and ground magnetometer observations, *J. Geophys. Res.*, **95**, 1061-1071, 1990.

Robinson, R. M., R. R. Vondrak, K. Miller, T. Dabbs, and D. Hardy, On the calculation of conductances from the flux and energy of precipitating electrons, *J. Geophys. Res.*, **92**, 2565-2570, 1987.

Ruohoniemi, J. M., R. A. Greenwald, K. B. Baker, J. P. Villain, and M. A. McCready, Drift motions of small-scale irregularities in the high-latitude *F* region: An experimental comparison with plasma drift motions, *J. Geophys. Res.*, **92**, 4553-4564, 1987.